Behavior of Diphtheria Toxin T Domain Containing Substitutions That Block Normal Membrane Insertion at Pro345 and Leu307: Control of Deep Membrane Insertion and Coupling between Deep Insertion of Hydrophobic Subdomains†

Gang Zhao and Erwin London*

Department of Biochemistry and Cell Biology and Department of Chemistry, Stony Brook University, State University of New York, Stony Brook, New York 11794-5215

Received October 27, 2004; Revised Manuscript Received December 30, 2004

ABSTRACT: Diphtheria toxin T domain aids the translocation of toxin A chain across membranes. T domain has two hydrophobic layers/subdomains that can insert deeply into membranes: helices TH8 and 9, which form a transmembrane hairpin, and helices TH5−7, which form a nonclassical, nontransmembrane structure. Substitutions were made at Pro345, a residue located near the turn between TH8 and 9. P345 is critical for toxicity and pore formation by the T domain. Fluorescence methods showed that hairpin-disrupting Gly or Glu substitutions at 345 did not insert into lipid bilayers as deeply as the wild-type protein, and consistent with previous studies, these mutations reduced pore formation activity as assayed by a novel biotin−streptavidin-based influx assay. Introducing Pro at positions 347 or 353 not only failed to compensate for substitutions at P345, but also they further disrupted deep insertion and/or pore formation. Substitution of P345 with Asn, a residue that promotes helical hairpin formation almost as well as Pro, resulted in somewhat more normal insertion and pore formation than other substitutions. Importantly, a P345E substitution disrupted deep insertion of TH5−7. This suggests that TH8 and 9 and TH5−7 undergo some sort of coordinated insertion into the lipid bilayer and/or that the membrane-inserted T domain has a distinct tertiary structure in which TH5−7 interact with TH8 and 9 instead of consisting of noninteracting hydrophobic segments. Intriguingly, a L307R substitution in TH6, which disrupted deep insertion of TH7, had only a weak effect on pore formation and deep insertion of TH8 and 9. This suggests that the TH8 and 9 region can insert independently of TH5−7 to some degree and that TH8 and 9 insertion may occur early in T-domain insertion.

Diphtheria toxin (DT)[1] is a pathogenic protein synthesized by *Corynebacterium diphtheriae* as a single polypeptide (MW, 58 kDa). Protease converts DT into its active form, which consists of two fragments or chains, A and B, linked by a disulfide bond. The crystal structure of DT shows that it has three distinctive domains (*1*, *2*). The catalytic domain is equivalent to the A chain, while the B chain contains two domains: the transmembrane (T) domain and the receptor-binding (R) domain. DT enters endosomes by receptor-mediated endocytosis. The low pH in endosomes triggers partial unfolding of the whole DT and T domain such that the T domain becomes more hydrophobic and penetrates the endosome membrane (*3*−*6*). The A chain is then translocated across the endosomal membrane. After release into the cytoplasm, which may be aided by cytosolic factors (*7*), the A chain inactivates elongation factor-2 by ADP ribosylation and thereby shuts down the protein synthesis pathway.

The largely α-helical T domain has been found to play a crucial role in membrane insertion and translocation (*3*, *8*−*12*). Although the mechanism by which the T domain aids translocation is unknown, its pore-forming ability and interactions with partly unfolded A chain are likely to be important aspects of its role in translocation (*9*−*13*). The crystal structure of DT showed that the helices (TH1−9) of the T domain are arranged into three layers or subdomains (*1*, *2*). The first layer consists of helices TH1−4, which are hydrophilic. The second layer is composed of helices TH5−7, which are somewhat hydrophobic. Helices TH8 and 9 form the third layer, which is the most hydrophobic region within DT. All three layers may be indispensable to T-domain function. One group has reported that, when a single helix-breaking proline residue is introduced into any

† This work was supported by NIH Grant GM31986.

* To whom correspondence should be addressed. Telephone: (631) 632-8564. Fax: (631) 632-8575. E-mail: erwin.london@stonybrook.edu.

[1] Abbreviations: 10-DN, 10-doxylnonadecane; BODIPY, 4,4-difluoro-5,7- dimethyl-4-bora-3a,4a-diaza-*s*-indacene; BODIPY-IA, (*N*-(4,4-difluoro-5,7-dimethyl-4-bora-3a,4a-diaza-*s*-indacene-3-yl)methyl)iodoacetamide; BODIPY-SA, BODIPY-labeled streptavidin; DMoPC, dimyristoleoylphosphatidylcholine; DOPC, dioleoylphosphatidylcholine; DOPG, dioleoylphosphatidylglycerol; DT, diphtheria toxin; DTT, dithiothreitol; HSA, human serum albumin; IPTG, isopropyl-1-thio-β-D-thiogalactopyranoside; LUV, large unilamellar vesicle; P state, partially/shallowly inserted T-domain state; rhodamine-DHPE, *N*-lissamine rhodamine B-1,2-dihexadecanoyl-*sn*-glycero-3-phosphoethanolamine; SDS−PAGE, sodium dodecyl sulfate−polyacrylamide gel electrophoresis; SUV, small unilamellar vesicle; T domain, diphtheria toxin "transmembrane" domain; TM, transmembrane; TM state, deeply inserted T-domain state in which TH8 and TH9 form a transmembrane structure.

10.1021/bi047705o CCC: $30.25
Published on Web 02/17/2005

one of the three layers, the toxin loses its toxicity and shows abnormal channel properties (*14*). Helices TH8 and 9 are of particular importance. They are critical for pore formation by the T domain, and mutations that disrupt their insertion into membranes also block translocation (*15*−*19*). Several studies showed that TH8 and 9 form a stable transmembrane (TM) hairpin at low pH (*3*, *6*, *8*, *18*, *20*−*25*). Using fluorescence techniques, we previously demonstrated that under some conditions a conformation forms in which TH8 and 9 lie close to the membrane surface (partially inserted or P state), while under other conditions, they insert more deeply and span the membrane bilayer (TM state) (*4*, *13*, *26*). In a more recent study, we found that when TH8 and 9 undergo the P to TM transition the hydrophobic TH5−7 subdomain also inserts deeper into the lipid bilayer, although not in a TM conformation (*27*, *28*).

In vitro mutagenesis has been used to identify some functionally important T-domain residues (*16*−*19*). One such residue is proline 345 (P345) (*17*, *19*), a residue near the tight loop found between TH8 and TH9 in the crystal structure of the native (water-soluble) conformation. Substitutions for P345 abolish both toxicity and normal pore formation (*17*, *19*). Interestingly, prolines at similar positions exist in several proteins with T-domain-like structures, e.g., proline 168 in the C domain of colicin A and proline 168 in Bcl-2 (*29*, *30*), suggesting a general role for proline in the loop of hydrophobic helical hairpins in this class of proteins. Consistent with this hypothesis, such a proline was shown recently to modulate the mitochondrial targeting and apoptotic activity of Bax (*31*).

In this work, several substitutions were introduced at position 345, and their effects on the conformations of helices TH5, 7, 8, and 9 were assessed by fluorescence techniques (*4*, *26*). The results indicate that proline at position 345 is important for maintaining the normal membrane insertion of both the TH8 and 9 and TH 5−7 segments and that these segments are likely to interact when T domain is in its deeply inserted conformation.

EXPERIMENTAL PROCEDURES

Materials. Dioleoylphosphatidylcholine (DOPC), dimyristoleoylphosphatidylcholine (DMoPC), and dioleoylphosphatidylglycerol (DOPG) were purchased from Avanti Polar Lipids (Alabaster, AL). Lipid concentrations were determined by dry weight. *N*-[(4,4-Difluoro-5,7-dimethyl-4-bora-3a,4a-diaza-*s*-indecene-3-yl)methyl]iodoacetamide (BODIPY-FL C1-IA, BODIPY-IA), monochlorobimane, rabbit anti-BODIPY-FL IgG, BODIPY-labeled streptavidin, and N-lissamine rhodamine B-1,2-dihexadecanoyl-*sn*-glycero-3-phosphoethanolamine (rhodamine-DHPE) were obtained from Molecular Probes (Eugene, OR). Human serum albumin (HSA) was purchased from Worthington Biochemical (Lakewood, NJ). *Pfx* polymerase, custom oligonucleotides, and DNA modification enzymes were from Invitrogen (Rockville, MD). pET-28a plasmid was from Novagen (Madison, WI). Lysozyme from chicken egg white was purchased from Sigma (St. Louis, MO). All other chemicals were reagent-grade.

PCR-Based Mutagenesis. DNA coding for DT T domain (residues 202−378) from the pET-15b-T plasmid (*23*) was subcloned into pET-28a plasmid between *Nde*I and *Eco*RI (pET-28a-T) to optimize expression [T domain expressed from this construct, which includes a 6× His-tag extension (*26*), was defined as wild-type T domain]. The pET-28a-T plasmid was used as a template for further mutagenesis. A two-step PCR approach was used to make the mutations. Complementary 5′ and 3′ mutation-containing primers (mutation primers), usually 30−40 base pairs long with a mutation in the middle, were designed based on the DNA sequence. PCR was carried out on an Eppendorf Mastercycler Personal PCR System using the high-fidelity *Pfx* polymerase.

In the first step of the PCR reactions, the T7 promoter primer/3′-mutation primer set was used to amplify the 5′ half of the mutant DNA and the 5′-mutation primer/T7 terminator primer set was used to amplify the 3′ half of the DNA. The products from both reactions were agarose-gel-purified and combined as templates in the second PCR step, in which the full-length DNA bearing the mutation was synthesized using the T7 promoter and terminator primers. The full-length DNA was digested with *Nde*I and *Eco*RI and ligated into linearized pET-28a vector. The ligation product was transformed into competent *Escherichia coli* strain XL-1 Blue cells by electroporation and selected against kanamycin on agar plates. The T-domain DNA insertions were sequenced to confirm the mutations and exclude cloning artifacts (Proteomics Center, Stony Brook University, NY).

Expression and Purification of the T Domain. Proteins were expressed and purified using the pET system from Novagen. To express proteins, the appropriate plasmid was transformed into *E. coli* BL21(DE3) competent cells by heat shock. A single colony was picked to inoculate 20 mL of Luria−Bertani (LB) media containing 50 μg/mL kanamycin. The media was grown overnight at 37 °C with shaking. The overnight culture was transferred into 2 L of LB media containing 50 μg/mL kanamycin. The culture was incubated at 37 °C with shaking until its optical density at 600 nm reached ∼0.5−0.6. Isopropyl-1-thio-β-D-thiogalactopyranoside (IPTG) was then added to a final concentration of 1 mM, and incubation was continued for 3 h to induce protein expression. The induced cells were collected by centrifugation and stored overnight at −80 °C. The next day the pellet was mixed with 500 mL of 1× binding buffer (20 mM Tris-HCl at pH 8.0 and 100 mM NaCl), repelleted, and after removal of the supernatant, resuspended in 40 mL of 1× binding buffer containing 100 μg/mL lysozyme. The cells were agitated at room temperature for 30 min and then disrupted by sonication on ice with a probe sonicator (Model W-220F cell disruptor, Heat System-Ultrasonics, Plainview, NY) until the solution was no longer viscous. The resulting homogenate was centrifuged at 12000*g* at 4 °C for 20 min. The supernatant (soluble cell extract) was saved for purification.

The induced proteins, which contained the N-terminal 6× His tag from pET28a, were purified using a TALON Metal Affinity Resin from Clontech (Palo Alto, CA). A total of 1 mL of TALON beads was batch-washed twice with 10 mL of 1× binding buffer for 5 min. After each addition of buffer, the beads were pelleted at 2000 rpm using a tabletop centrifuge and the supernatants were decanted. The soluble cell extract was mixed with the washed beads and gently agitated at room temperature for 40 min to allow the 6× His-tagged protein to bind to the resin. The protein/resin complex was washed with 30 mL of 1× binding buffer, as

described above. The resin was then transferred to a 10-mL gravity-flow column. The column was washed with 5 mL of 1× binding buffer 3 times and then eluted with 5 mL of elution buffer (1× binding buffer plus 100 mM imidazole). To further purify and concentrate the protein, the eluted sample was subjected to FPLC using a Source Q anion-exchange column. The sample was diluted to 50 mL with 20 mM Tris-HCl at pH 8 (buffer A) and then loaded onto the Source Q column equilibrated with buffer A. The column was then eluted at a rate of 0.5 mL/min with an increasing salt gradient (20 mM Tris-HCl at pH 8.0 and 0−0.5 M NaCl). The purified T domain eluted in fractions with about 300 mM NaCl. The collected fractions were subjected to SDS−PAGE to verify that at least 90% purify was obtained. The protein concentration was determined using the Bio-Rad (Hercules, CA) protein assay (*32*). Usually more than 5 mg of purified protein was obtained from a 2 L culture. The purified T domain was stored at −20 °C in the FPLC buffer in which it had eluted.

Fluorescence Labeling of the T Domain. The T domain was labeled with the thiol-reactive fluorescent probes BODIPY-IA and monochlorobimane as described previously (*27*). To ensure efficient labeling, 200 μg of protein in 1 mL was reduced with 100 mM dithiothreitol (DTT) for 2 h at room temperature and then dialyzed overnight against 4 L of TBS buffer (10 mM Tris-HCl at pH 8.0 and 150 mM NaCl) with no buffer change prior to labeling. A small aliquot containing either BODIPY-IA dissolved in dimethyl sulfoxide or monochlorobimane dissolved in ethanol (in both cases using about 20 mM stock solutions) was added to give a 10:1 probe/protein mole ratio. The reaction mixture was protected from light and slowly agitated at room temperature for 1 h. The unbound fluorescent probe was removed by overnight dialysis against 4 L of TBS with one change of buffer. Labeling efficiency was checked by fluorescence intensity and compared to the background labeling of the wild-type protein (which lacks cysteine). Fluorescence intensities of the labeled mutants were at least 10 times over the background labeling.

Fluorescence Measurements. Fluorescence was measured at room temperature on a Spex tau-2 Fluorolog Spectrofluorimeter operating in steady-state mode using 10 mm excitation path-length and 4 mm emission path-length semi-micro quartz cuvettes. The excitation and emission slits were set to 2.5 and 5.0 mm (4.3 and 8.6 nm bandwidth), respectively. Bimane fluorescence was measured with an excitation wavelength of 380 nm. Emission spectra were collected at 1 nm/s from 420 to 500 nm. BODIPY fluorescence intensity was measured with an excitation wavelength of 488 nm and emission wavelength of 516 nm. Trp fluorescence emission intensity of unlabeled protein was measured at 330 and 350 nm with an excitation wavelength of 280 nm. In all cases, background intensities from samples lacking protein were subtracted from the intensities measured in samples containing the T domain.

Lipid-Binding Experiments. The ability of the T domain to associate with lipid vesicles was assessed by the blue shift of its native tryptophan fluorescence upon binding to the lipid (*4*). A total of 3.5 μg of unlabeled T domain was diluted to 700 μL with Tris-acetate buffer (6.7 mM Tris-HCl, 167 mM acetate, and 150 mM NaCl at pH 4.5) and incubated at room temperature for 20 min. Then, aliquots of 10 mM 70% DOPC/30% DOPG (mol/mol) small unilamellar vesicles (SUVs), prepared in Tris-acetate buffer at pH 4.5 by sonication as previously described (*26*), were titrated into the protein solutions. Tryptophan fluorescence was measured 10 min after each addition. The ratio of emission intensities at 330 and 350 nm was used to detect the fluorescence spectra shifts that accompany binding to lipid vesicles (*4*).

Preparation of the Model Membrane-Incorporated T Domain and Analysis of Fluorescence Properties. Samples containing T domain were incorporated into SUVs at pH 4.5. SUVs composed of 70% DOPC/30% DOPG or of 70% DMoPC/30% DOPG (mol/mol), with a final concentration of 10 mM lipid, were prepared by sonication in Tris-acetate buffer at pH 4.5 as previously described (*26*). In a typical sample, a 14 μL aliquot of SUVs was added to 678−682 μL of Tris-acetate buffer at pH 4.5. To this, 0.7 μg of fluorescently labeled T domain (4−8 μL of stock solution) was added with agitation. The final volume of each sample was 700 μL. The samples were incubated at room temperature for 20 min before fluorescence was measured. For the bimane-labeled samples, fluorescence emission spectra were measured as described above. For the BODIPY-labeled samples, anti-BODIPY quenching experiments were performed as described previously (*27*). The samples were prepared as described above, and the BODIPY fluorescence intensity was measured before 40 μL of anti-BODIPY antibody (3 mg/mL commercial stock solution) was added. After incubation for 20 min, the BODIPY fluorescence intensity was measured again and quenching values were calculated.

To examine the effects of high T-domain concentrations or the presence of HSA upon T-domain conformation, bimane- or BODIPY-labeled T domain was incorporated into 70% DOPC/30% DOPG SUVs at pH 4.5 as described above. After incubation for 10 min, an aliquot containing unlabeled wild-type T domain or HSA was added to give a final concentration of either 10 μg/mL unlabeled wild-type T domain (3−6 μL aliquot from a stock solution dissolved in TBS) or 5 μg/mL HSA (3.5 μL from a 1 mg/mL solution of HSA dissolved in water). In one experiment, an aliquot of unlabeled T domain containing the P345E and A356C mutations was used in place of the wild type. After incubation for 10 min, fluorescence was measured as described above.

The data from these experiments were used to evaluate the degree of insertion of individual fluorescently labeled T-domain residues. The T domain was previously shown to adopt the P conformation in DOPC-containing SUVs (*4*, *26*). To reliably evaluate the ability to form the TM conformation, three cases shown previously to induce formation of the TM conformation were investigated: insertion into DMoPC-containing SUVs, addition of a high concentration of wild-type T domain to T domain inserted into DOPC-containing vesicles, or addition of a molten-globule state protein (e.g., HSA at low pH) to T domain inserted into DOPC-containing vesicles (*4*, *26*, *27*). The bimane emission λ_{max} values and the BODIPY quenching values under TM conditions were averaged. The difference between the λ_{max} values in the P state and TM-state-inducing condition values was also calculated. For BODIPY fluorescence, the loss of BODIPY quenching upon switching from P state to TM-state-inducing conditions was calculated from the expression $(\%Q_P - \%Q_{TM})/\%Q_P \times 100\%$, where $\%Q_P$ and $\%Q_{TM}$ are

the percent quenching of BODIPY fluorescence intensity upon antibody addition in P conditions and the average of TM conditions, respectively. Notice that a high percent quenching corresponds to a high degree of exposure to aqueous solution.

Relative Depth of Bimane-Labeled Residues. Dual quenching experiments were performed to assess the depth of bimane residues in bilayers more directly. In this method, fluorescence quenching by molecules in aqueous solution and by quenchers embedded in the lipid bilayer is compared (*33*, *34*). Iodide ion was used as the aqueous quencher of bimane fluorescence and 10-doxylnonadecane (10-DN) was used as the membrane-bound quencher. SUVs were prepared with the ethanol dilution method (*35*, *36*). Mixtures of lipids dissolved in chloroform were dried under a nitrogen stream and then with high vacuum for 1 h. The lipid film was dissolved with 10 μL of 100% ethanol. Then, 680 μL Tris-acetate buffer at pH 4.5 was added, and the samples were vortexed to disperse the lipid mixture and form SUVs. The final samples contained either: (1) 140 μM DOPC/60 μM DOPG with or without 40 μM 10-DN or (2) 140 μM DMoPC/60 μM DOPG with or without 31.2 μM 10-DN [The concentration of 10-DN was normalized to the number of carbon atoms in the PC acyl chains to give roughly the same concentration of quencher groups per unit hydrophobic volume (*33*)]. Next, 0.7 μg of bimane-labeled T domain adjusted to 10 μL (with TBS) was added with agitation. The samples were incubated at room temperature for 20 min before fluorescence was measured. Bimane fluorescence in samples with 10-DN (F_{10-DN}) was then compared to samples without 10-DN (F_0). For iodide-quenching experiments, bimane-labeled proteins were incorporated into SUVs prepared as above without 10-DN. Bimane fluorescence was measured both before (F_0) and after (F_{I^-}) the addition of 45 μL of 1.7 M KI solution containing 0.85 mM $Na_2S_2O_3$ freshly prepared (fluorescence values in the latter samples were corrected for dilution). The quenching (Q) ratio, defined as $((F_0/F_{10-DN}) - 1)/((F_0/F_{I^-}) - 1)$, was then calculated. A higher quenching ratio is indicative of a deeper residue location in the bilayer.

Pore-Formation Experiments. T-domain-induced pore formation was measured by a novel assay in which the increase in the BODIPY fluorescence of vesicle-entrapped BODIPY-labeled streptavidin (BODIPY-SA) is used to detect biocytin influx. LUVs with trapped BODIPY-SA were prepared by detergent dialysis (*37*). A lipid mixture containing 70% DOPC/30% DOPG and 0.02% rhodamine-DHPE dissolved in chloroform was dried under a nitrogen stream and then high vacuum for 1 h. The dried lipid film was suspended to a lipid concentration of 10 mM with phosphate-buffered saline (PBS, 1 mM KH_2PO_4, 10 mM Na_2HPO_4, 137 mM NaCl, and 2.7 mM KCl at pH 7.4) containing 200 μg/mL BODIPY-SA and 20 mg/mL octyl glucoside in a final volume of 1 mL. The mixture was dialyzed against 2 L of PBS overnight with one change of dialysis buffer. Untrapped BODIPY-SA was separated from vesicle-trapped BODIPY-SA on a Sepharose 4B-CL gel-filtration column (0.5 $\times$ 40 cm) at room temperature. Samples were eluted using PBS, and the fractions containing the LUVs were pooled. BODIPY and rhodamine fluorescences were used to calculate the final BODIPY-SA and lipid concentrations, which were around 15 μg/mL and 5 mM, respectively. Trapping efficiencies were between 7 and 10%. For the pore formation experiments, LUVs with entrapped BODIPY-SA were diluted to 790 μL with Tris-acetate buffer to a final lipid concentration of 50 μM. The BODIPY-SA concentration in the diluted samples was between 0.1 and 0.15 μg/mL. A total of 0.35 μg of T domain adjusted to 5 μL with TBS was added to the samples. After incubation at room temperature for 20 min, biocytin was added to a final concentration of 24-fold over the mole concentration of BODIPY-SA (4−7 μL of 7 μM biocytin dissolved in water) and BODIPY fluorescence intensities were monitored for 1 h.

RESULTS

T-Domain Mutants. Site-directed mutation was used to prepare T domains with substitutions for residue P345 in helix TH8 or for residue L307 in helix TH6. In the former case, proteins were also prepared with a new Pro at residue 347 at the end of helix TH8 or residue 353, which is at the start of helix TH9. Substitutions at P345 were also combined with insertion of four Gly residues in the hydrophilic loop between helices TH7 and 8. To probe the effects of these mutations, single fluorescently labeled Cys substitutions were introduced at positions in helix TH5, 7, or 9 at which they do not prevent deep T-domain membrane insertion (*26*, *27*): residues 280, 311, and 356, respectively. Labels on these residues are sensitive to changes in the local degree of membrane insertion (*4*, *26*, *27*). In all cases, proteins carrying mutations maintained normal binding to lipid vesicles and the normal ability to insert into lipid vesicles, as judged by the blue shift in T-domain native Trp fluorescence upon association with lipid vesicles at low pH (*4*) and its dependence upon lipid concentration (data not shown).

Effects of Substitutions at Position 345 on the Behavior of the TH8 and 9 Hairpin: Evaluation of Conformation from Bimane Fluorescence. First, the effects of P345G and P345E mutations, known to alter the behavior of the model membrane-inserted T domain (*17*, *19*), were examined. Using a fluorescence label at position 332, Zhan et al. showed that P345E mutation blocks membrane insertion to some degree (*19*) but did not specify the degree to which insertion was altered, whether conformational changes in P345G and P345E mutations are similar or whether blocked insertion could be overcome by altering experimental conditions. Thus, we reinvestigated the degree to which these mutations disrupt normal deep insertion.

To study membrane penetration by the T-domain mutants, their conformation under conditions (low concentrations of T domain in DOPC-containing SUV) in which the wild-type T domain forms the P state, which only shallowly penetrates membranes (*4*, *26*, *27*), was compared to that under three separate conditions that ordinarily give rise to the deeply inserting TM state (in which helices TH8 and 9 form a TM hairpin). These conditions are insertion into SUV with a thin bilayer width (DMoPC-containing vesicles), interaction with a molten-globule protein (e.g., HSA at low pH), or when there is a high T domain/lipid ratio (high T domain concentration, HT) (*4*, *26*).

Membrane penetration was first evaluated via the fluorescence emission of bimane attached to Cys at position 356

Table 1: Effects of P345 Mutations on TH8 and 9 Conformation as Assessed by the Emission λ_{max} of Bimane Attached to Residue 356[a]

protein	$\lambda_{max,P}$ DOPC	$\lambda_{max,TM}$ DMoPC	$\lambda_{max,TM}$ HSA	$\lambda_{max,TM}$ HT	$\lambda_{max,TM}$ average	$\Delta\lambda_{max}$	% wild type $\Delta\lambda_{max}$
A356C (wild type)	468.0	459.5	460.0	459.0	459.5	8.5	100.0
P345E/A356C	468.0	462.5	465.0	463.5	463.7	4.3	51.0
P345G/A356C	468.0	462.5	464.5	462.5	463.2	4.8	56.9
P345N/A356C	467.5	461.5	464.5	462.5	462.8	4.7	54.9
P345E/V347P/A356C	468.5	466.5	467.0	465.0	466.2	2.3	27.5
P345E/I353P/356C	467.0	462.5	462.0	462.0	462.2	4.8	56.9
P345G/I353P/A356C	467.5	463.0	462.5	460.5	462.0	5.5	64.7

[a] Samples contained 1 μg/mL T domain inserted into 70% DOPC (or DMoPC when explicitly noted)/30% DOPG SUV with a lipid concentration of 200 μM dispersed in Tris-acetate buffer at pH 4.5. Sites of mutations are shown in the left column. Bimane label attached to Cys introduced at residue 356 was used to probe TH9 conformation. Addition of excess T domain (high T domain concentration, HT) and HSA are described in the Experimental Procedures. λ_{max} values under the TM-state-inducing conditions (DMoPC, HSA, and HT) were defined as $\lambda_{max,TM}$. They were averaged and subtracted from the values under the P-state-forming conditions ($\lambda_{max,P}$) to calculate $\Delta\lambda_{max}$. To calculate % wild type $\Delta\lambda_{max}$, the $\Delta\lambda_{max}$ numbers for T domain mutants were normalized to that of the more "wild-type" protein bearing only the Cys mutation (Note that this protein is distinct from the true wild type and that in the HT samples the unlabeled T domain used was the true wild type). Results shown are the average values of duplicate samples. Wavelength maxima were generally reproducible within $\pm$1 nm.

in helix TH9. Bimane fluorescence of labeled Cys 356 has previously been shown to be red-shifted when the T domain is in the P conformation and blue-shifted in the TM conformation (*4*, *26*). Table 1 shows that bimane-labeled Cys 356 shows red-shifted fluorescence under conditions in which the surface conformation ordinarily predominates both with wild-type P345 and in mutants containing a P345E or P345G mutation. This suggests that these mutations at position 345 do not greatly affect the P-state conformation. In contrast, under all three conditions in which the TM state normally forms, the blue shift in bimane fluorescence was significantly less (averaging about half of the normal shift) for the T domain with P345E or P345G mutations relative to that with a wild-type P345 residue. This suggests a partial disruption of deep membrane penetration by these mutations.

A key property of Pro in membrane proteins is its tendency to induce helical hairpin formation when placed in the middle of a long transmembrane segment (*38*). Monne et al. defined an experimental turn propensity scale for all 20 amino acids, ranking their abilities to induce helical hairpin formation in an otherwise TM segment (*39*). As expected, Pro had the highest turn propensity. Thus, a structural function of P345 may be to help helices TH8 and 9 form a hairpin structure. Monne et al. found Asn to be the second most efficient helix hairpin inducer (*39*). To try to examine whether the turn-inducing propensity of Pro was critical for proper TM-hairpin insertion of TH8 and 9, we compared the behavior of the T domain with a P345N mutation to that of the T domain with P345E and P345G mutations, both of which involve substitutions that promote turn formation to a lesser degree (*39*). Monne et al. also showed that the position of Pro in a long TM segment affected its hairpin-inducing ability, with the highest turn propensity requiring placement in the middle of the segment. To test whether the influence of Pro upon the helices TH8 and 9 is strongly position-dependent, we shifted the proline to positions 347 and 353, positions about as close as residue 345 to the center of the TH8 and 9 hydrophobic segment. Neither the P345N mutation (however, see below) nor the repositioned Pro residues rescued the normal P to TM conformational transition as judged by bimane fluorescence (Table 1). In fact, introduction of a Pro at position 347 further inhibited the blue shift under TM-state-favoring conditions.

Effects of Substitutions at Position 345 on the Behavior of the TH 8 and 9 Hairpin: Evaluation of Conformation from Anti-BODIPY Antibody Binding. Anti-BODIPY antibody binding to BODIPY labels attached to residue 356 was used as a second method to evaluate membrane penetration of TH9. Antibody binding to exposed BODIPY-labeled residues quenches BODIPY fluorescence by a factor of 2−3 (*4*, *26*, *27*). Previous studies demonstrated that BODIPY groups attached to residues within the hydrophobic helices of the T domain become up to 2-fold less reactive with externally added anti-BODIPY antibody when the residues to which they are attached become buried within the lipid bilayer in the TM state [The residual binding of antibodies to membrane-penetrating residues may be due to a subpopulation of T-domain molecules that do not insert deeply (*26*)]. As judged from this assay, T domains carrying the P345E and P345G mutations undergo only slightly less of a decrease in antibody binding upon the P to TM transition as does the "wild-type" protein (Table 2). In other words, TH9 in these mutants appears to be slightly less buried than the wild-type protein in the TM state.

As also shown in Table 2, the T domain with the P345N mutation exhibited antibody-binding behavior even more similar to that of the wild-type protein in the TM state. However, because the effect of the P345E and P345G mutations on antibody binding is relatively small, it is not clear whether the difference between their behavior and that of P345N is significant. Combining P345E or P345G with the introduction of Pro at 347 or 353 further inhibited the loss in antibody reactivity (i.e., further inhibited deep insertion) accompanying the P to TM transition. This suggests that the introduction of Pro at both of these positions further disrupts formation of the normal TM state.

Effects of Substitutions at Position 345 on the Behavior of the TH8 and 9 Hairpin: Effect on Pore Formation by the T Domain. T-domain pore formation is associated with normal insertion and the ability to translocate the A chain (*9*−*12*, *40*). Because proper insertion of TH8 and 9 is critical for pore formation (*41*), the effect of mutations at position 345 upon pore formation was also used to evaluate the effect of mutations upon TH8 and 9 insertion. For pore formation experiments, we developed a powerful assay measuring the influx of biocytin (ϵ-biotinyl-lysine) into the lumen of

Table 2: Effects of P345 Mutations on TH8 and 9 Conformation as Assessed by the Antibody Quenching of the Fluorescence of BODIPY Attached to Residue 356[a]

	$\%Q_P$	$\%Q_{TM}$			$\%Q$				
protein	DOPC	HSA	DMoPC	HT	HSA	DMoPC	HT	average % ΔQ	average % wild type ΔQ
A356C (wild type)	49.5 ± 8.8	33.7 ± 1.1	22.8 ± 5.6	11.5 ± 1.0	31.9 ± 5.8	53.9 ± 16.4	76.8 ± 15.2	54.2	100.0
P345E/A356C	37.1 ± 3.1	29.6 ± 1.8	13.8 ± 6.3	13.6 ± 1.7	20.2 ± 2.1	62.8 ± 29.1	63.3 ± 9.5	48.8	90.0
P345G/A356C	40.9 ± 2.9	29.1 ± 0.8	22.7 ± 2.3	14.0 ± 1.1	28.9 ± 2.2	44.5 ± 5.5	65.8 ± 7.0	46.4	85.5
P345N/A356C	47.7 ± 6.6	30.9 ± 4.0	23.0 ± 9.1	15.4 ± 2.4	35.2 ± 6.7	51.8 ± 21.7	67.7 ± 14.1	51.6	95.1
P345E/V347P/A356C	42.6 ± 0.4	33.1 ± 2.9	27.7 ± 8.2	26.1 ± 2.3	22.3 ± 2.0	35.0 ± 10.4	38.7 ± 3.4	32.0	59.0
P345E/I353P/A356C	52.9 ± 0.8	44.1 ± 6.6	23.5 ± 5.5	31.6 ± 4.0	16.6 ± 2.5	55.6 ± 13.0	40.3 ± 5.1	37.5	69.2
P345G/I353P/A356C	52.8 ± 0.8	44.4 ± 5.0	39.2 ± 0.4	27.2 ± 3.5	15.9 ± 1.8	25.8 ± 0.5	48.5 ± 6.3	30.1	55.4

[a] Sample composition as in Table 1. Sites of mutations are shown in the left column. BODIPY label attached to Cys introduced at residue 356 was used to probe TH9 conformation. The percent quenching of BODIPY fluorescence intensity under the P state-forming conditions ($\%Q_P$) and the percent quenching under the TM-state-forming conditions ($\%Q_{TM}$) were used to calculate $\%\Delta Q$, using the formula $\%\Delta Q = ((\%Q_P - \%Q_{TM})/\%Q_P) \times 100\%$. To calculate % wild type ΔQ, the $\%\Delta Q$ for a mutant was normalized to that of the protein bearing only the Cys mutation (wild type). Results shown are for the average of duplicate samples and their range.

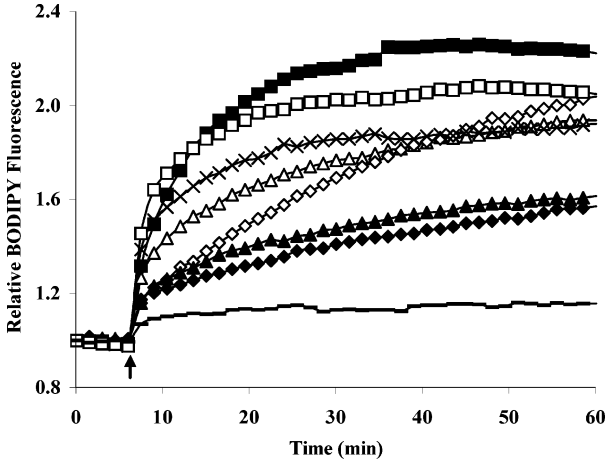

FIGURE 1: T-domain-induced biocytin leakage into LUVs at pH 4.5. Samples containing LUV (50 μM lipid) loaded with BODIPY-SA and containing 0.5 μg/mL bound T domain proteins were preincubated for 20 min in Tris-acetate buffer at pH 4.5 before biocytin was added (arrow). Fluorescence was recorded every 90 s for 1 h. The initial fast increases in the BODIPY fluorescence were partially due to a residual amount [~6% as estimated by the BODIPY fluorescence increase when biocytin was added at neutral pH (not shown)] of BODIPY-SA outside of the LUVs. A small contribution from T-domain-induced leakage of BODIPY-SA from the LUV lumen cannot be ruled out. Results shown in each case are the average of at least two experiments, each of which gave similar results. Only fluorescence intensity during the last 6 min of the preincubation step is shown. All proteins contained the A356C mutation. Symbols for the T domain: ■, wild type at position 345; △, P345E; ◇, P345G; ×, P345N; ◆, P345G/I353P; ▲, P345E/I353P; □, L307R; and —, no T domain control.

vesicles. Influx was detected by the increase in the BODIPY fluorescence of vesicle-entrapped BODIPY-SA, which is too large to escape from vesicles at the T domain concentrations used (*42*). Biotin binding to BODIPY-SA displaces the BODIPY group from the biotin-binding pocket, in which BODIPY fluorescence is quenched (*43*). Advantages of this assay are described in the Discussion.

Figure 1 compares pore formation by the wild-type T domain and various mutants. The P345E mutation resulted in reduced pore activity (as judged by the rate of influx over the first 10 s) relative to the wild type at position 345, in agreement with previous studies (*19*). The P345G mutation resulted in a slightly lesser degree of pore formation than P345E. The T domains with either P345E plus I353P mutations or P345G plus I353P mutations showed a further reduction in pore activity relative to that for P345E or P345G mutants, in agreement with their above-described stronger disruption of insertion as detected by anti-BODIPY antibody binding. In contrast, the T domain with the P345N mutation gave a rate of biocytin influx close to that observed for the wild-type protein.

Overall, the conclusions derived from the effect of mutations upon pore disruption agree well with those from bimane fluorescence and anti-BODIPY antibody binding. The exact extent of the deleterious effects of P345E and P345G substitutions depends on the assay chosen, although all three methods show that there is significantly impaired deep insertion of the hydrophobic helices TH8 and 9 subdomain in these mutants. All of the methods also agree that the necessity for a Pro at position 345 (and/or the deleterious effect of the introduction of Glu or Gly at position 345) is stringent in the sense that shifting the Pro to a nearby position does not overcome P345E or P345G mutations. Introduction of Pro at positions 347 or 353 only further disrupted proper insertion in the TM state (as judged by antibody binding, by bimane fluorescence for the P347 substitution, and by pore formation for the P353 substitution). In contrast, Asn at position 345 appears to be slightly better than Glu or Gly at allowing normal insertion.

Interactions Between Mutant and Wild-Type T Domains. High T domain concentrations within lipid bilayers promote the P to TM transition and increase the T domain pore size (*4*, *26*, *42*). In agreement with these studies, addition of the unlabeled wild-type T domain to the T domain that was wild type at position 345 and labeled on residue 356 promoted the P to TM transition, as judged by the large blue shift in bimane fluorescence and reduced antibody quenching (HT conditions, Tables 1 and 2). Similar results were observed upon the addition of the same concentration of unlabeled P345E mutant to wild-type protein labeled on residue 356. Bimane λ_{max} shifted from 467 to 459 nm and quenching by anti-BODIPY antibody decreased from 48.9 ± 2 to 27.4 ± 2.9%. However, adding the unlabeled wild-type T domain to the P345E mutant labeled on residue 356 did not induce formation of a wild-type TM conformation, as shown by a decreased blue shift and a lesser decrease antibody quenching relative to that observed when it was added to the T domain that was wild type at position 345 (see HT conditions, Tables 1 and 2).

Table 3: Effects of Mutations in T Domain Helix TH6 (L307R), at the C-Terminal End of Helix TH8 (P345E) and/or in the Loop Connecting TH7 to TH8 upon the Conformational Behavior of TH5 5, 7, and 9 Assessed by Bimane Emission λ_{max}[a]

		$\lambda_{max,TM}$					
protein	$\lambda_{max,P}$ DOPC	DMoPC	HSA	HT	$\lambda_{max,TM}$ average	$\Delta\lambda_{max}$	% Δ wild type λ_{max}
A280C (wild type)	474.0	464.5	466.0	466.0	465.5	8.5	100.0
A280C/P345E	469.0	467.0	466.5	467.5	467.0	2.0	23.5
A280C/319G4/P345E	472.0	465.0	465.5	466.5	465.7	6.3	74.5
G311C (wild type)	467.5	461.5	461.5	460.5	461.2	6.3	100.0
G311C/P345E	468.0	464.0	464.5	463.0	463.8	4.2	65.8
G311C/319G4/P345E	467.5	462.0	462.5	463.0	462.5	5.0	79.0
L307R/G311C	466.0	465.0	464.5	465.0	464.8	1.2	18.4
A356C (wild type)	468.0	459.5	460.0	459.0	459.5	8.5	100.0
L307R/A356C	468.0	459.0	461.0	460.0	460.0	8.0	94.1

[a] Sample composition as in Table 1. Sites of mutations are shown in the left column. Bimane labels on Cys introduced at positions 280, 311, or 356 were used to probe the conformations of TH5, 7, and 9, respectively. In 319G4 protein, four consecutive Gly were inserted between residue 319 and 320. See footnote of Table 1 for other details.

Table 4: Effects of Mutations in T Domain Helix TH6 (L307R), at the C-Terminal End of Helix TH8 (P345E) and/or in the Loop Connecting TH7 to TH8 upon the Conformational Behavior of TH5 5, 7, and 9 Assessed by Antibody Quenching of BODIPY Fluorescence[a]

	Q_P	Q_{TM}			% ΔQ				
protein	DOPC	HSA	DMoPC	HT	HSA	DMoPC	HT	average % ΔQ	average % wild type ΔQ
A280C (wild type)	50.5 ± 1.0	39.0 ± 5.6	29.6 ± 7.4	19.7 ± 3.2	22.8 ± 3.3	41.4 ± 10.4	61.0 ± 10.0	41.7	100.0
A280C/P345E	53.0 ± 0.7	49.6 ± 0.4	37.4 ± 6.1	36.3 ± 3.3	6.4 ± 0.1	29.4 ± 4.8	31.5 ± 2.9	22.5	53.8
A280C/319G4/P345E	52.5 ± 2.4	37.4 ± 2.6	36.4 ± 3.9	35.9 ± 2.0	28.8 ± 2.4	30.7 ± 3.6	31.6 ± 2.3	30.3	72.8
G311C (wild type)	41.8 ± 4.4	19.4 ± 9.7	13.6 ± 4.6	5.4 ± 0.4	53.6 ± 27.4	67.5 ± 23.9	87.1 ± 11.2	69.4	100.0
G311C/P345E	45.2 ± 3.5	37.8 ± 0.7	17.9 ± 7.0	18.7 ± 4.0	16.4 ± 1.3	60.4 ± 24.1	58.6 ± 13.3	45.1	65.1
G311C/319G4/P345E	48.8 ± 5.8	33.8 ± 4.6	34.7 ± 4.2	31.5 ± 3.5	30.7 ± 5.6	28.9 ± 4.9	35.5 ± 5.8	31.7	45.7
L307R/G311C	41.7 ± 4.5	30.0 ± 3.8	19.7 ± 3.7	26.0 ± 0.0	28.1 ± 4.7	52.8 ± 11.4	37.6 ± 4.1	39.5	56.9
A356C (wild type)	49.5 ± 8.8	33.7 ± 1.1	22.8 ± 5.6	11.5 ± 1.0	31.9 ± 5.8	53.9 ± 16.4	76.8 ± 15.2	54.2	100.0
L307R/A356C	35.3 ± 0.4	17.7 ± 1.0	22.7 ± 1.2	17.6 ± 1.4	49.9 ± 2.9	35.7 ± 1.9	50.1 ± 4.0	45.2	83.4

[a] Sample composition as in Table 1. See footnotes of Tables 2 and 3 for other experimental details and calculations.

Mutational Analysis of Linkage Between Deep Membrane Insertion of Helices TH5−7 and Helices TH8 and 9. We recently found that, when helices TH8 and 9 undergo the P to TM conformational transition, helices TH5−7 undergo a conformational change from a shallow state to a deeper, although non-TM, state (*27*, *28*). However, these studies did not distinguish whether the TH8 and 9 and TH5−7 subdomains insert independently of each other or in a concerted manner. The P345 mutants were used to investigate the possible linkage between the insertion of these two hydrophobic regions. The behaviors of helices TH5 and TH7 in these mutants were studied by using single-labeled Cys at position 280 or 311, respectively. As shown in Table 3, in the presence of the P345E mutation, bimane-labeled residue 280 or 311 showed a smaller λ_{max} blue shift under conditions inducing the P to TM transition than the "wild type" T domain (bimane-labeled at residue 280 or 311 but with a Pro at position 345). Part of the inhibition for residue 280 represents an increased blue shift in the P state, implying that the P345E mutation affects the conformation at residue 280 in the P state as well as in the TM state. Analogous experiments with T-domain molecules BODIPY-labeled on Cys residues at position 280 and 311 showed the P345E mutation also inhibited the decrease in antibody binding at positions 280 and 311 upon inducing the P to TM transition (i.e., relative to the T domain with a Pro at 345) (Table 4). Thus, inhibiting deep insertion of the helices TH8 and 9 subdomain inhibits the deep insertion of the helices TH5−7 subdomain.

The reciprocal experiment was carried out to examine the effect of inhibiting deep insertion of helices TH5−7 upon insertion of the TH8 and 9 subdomain. To inhibit the insertion of the helices TH5−7, a positively charged residue was introduced into the center of the sequence encompassing hydrophobic helices TH6−7 by a L307R substitution. The insertion of helix TH9 was probed by fluorescently labeling a Cys at position 356. Control experiments (with Pro at position 345) confirmed that the L307R largely abolished deep insertion of helix TH7. The blue shift of bimane-labeled residue 311 upon formation of the TM state was almost totally lost in the presence of the L307R mutation (Table 3), while the loss of antibody-induced quenching associated with the P to TM state conformational change was reduced to about half of that seen with the wild-type protein (Table 4).

However, the deep insertion of helices TH8 and 9 in the TM state was not strongly affected by the L307R mutation. Using protein labeled on residue 356 showed that the blue shift in bimane fluorescence upon formation of the TM state was just about the same for the wild type at position 307 (Table 3), and there was only a small difference between the change in antibody-induced quenching associated with the change from P to TM conditions in the presence of L307R and that observed with the T domain that was wild type at position 307 (Table 4). These results are consistent with pore-formation experiments (Figure 1). The L307R mutant formed pores with an activity similar to those formed by the "wild type" protein.

Effect of the Loop Between Helices TH7 and TH8 Upon the Linkage Between Hydrophobic Subdomains. The interaction between the TH5−7 and TH8 and 9 subdomains could involve direct helix−helix interactions or instead reflect coupling of helix conformations because of a fixed confor-

mation within the hydrophilic loop connecting helix TH7 to helix TH8. To see if the 7−8 loop conformation was critical, four Gly residues were inserted between residues 319 and 320 to greatly increase loop flexibility. T domains with both the tetraGly insertion and P345E mutation and also bimane or BODIPY labeled on Cys at residues 280 or 311 showed that the tetraGly insertion neither restored "wild type" deep insertion of the helices TH5−7 region in the TM state nor totally abolished the deep insertion of helices TH5−7. Instead, they showed a partially blocked ability to form the normal TM state as judged both by bimane λ_{max} (Table 3) and anti-BODIPY antibody binding (Table 4). If the specific native loop conformation was required for allowing the deep insertion of helices TH5−7, then the tetraGly insertion should have fully abolished deep insertion of TH5−7. If the native loop conformation coupled the insertion of helices TH5−7 to helices TH8 and 9, but TH5−7 were capable of inserting fully independently of TH8 and 9, then the tetraGly insertion should have allowed wild-type deep insertion of TH5−7 in the presence of the P345E mutation. Neither of these behaviors was observed. This suggests that direct conformational coupling via the 7−8 loop is not critical for the interaction between TH5−7 and TH8 and 9 subdomains. However, there was a significant increase in the degree of membrane penetration by residue 280 in a P345E mutant containing the tetraGly insertion relative to that in the absence of the tetraGly insertion as judged by an increased bimane blue shift (Table 3) and decreased anti-BODIPY-induced quenching (Table 4). This suggests that the loop has some affect on TH5 behavior. In contrast, the tetraGly insertion had no consistent effect on insertion of residue 311 in TH7, suggesting that TH7 is less affected by the 7−8 loop conformation than TH5 (see Tables 3 and 4).

Measurement of the Depth of T-Domain Residues by Fluorescence Quenching. The fluorescence methods above do not directly measure membrane penetration depth, and inaccessibility of a residue to aqueous solution might reflect the degree of occlusion of residues from solution by other protein residues as well as the degree of burial within the lipid bilayer. However, we previously confirmed by fluorescence-quenching methods that the degree of burial within the lipid bilayer was the predominant factor in bimane fluorescence of, and BODIPY antibody binding to, labeled T-domain residues (*26*, *27*). Nevertheless, quenching studies were undertaken to confirm that this was also the case for the mutants in this study. To do this, quenching by iodide ion was used to evaluate bimane proximity to aqueous solution and quenching by 10-DN, a probe that inserts deeply within bilayers, was used to measure bimane proximity to the bilayer center (*33*, *34*). If a bimane has a shallow location in a bilayer, it will be strongly quenched by iodide and weakly quenched by 10-DN, while bimane deeply buried in the bilayer will be more heavily quenched by 10-DN and weakly by iodide. Thus, the ratio of 10-DN to iodide quenching reflects the relative depth of a bimane label in the bilayer, with a higher quenching ratio indicating a deeper location (*33*, *34*). We previously confirmed that the ratio of 10-DN quenching to that by an aqueous quencher reflects depth using synthetic TM helices (*33*) and labeled T-domain residues known to be shallowly or deeply inserted (*34*).

As shown in Figure 2, the depth of bimane-labeled residues at positions 311 and 356 was shallow (low ratio) in the P state and deeper in the TM state, in agreement with the assays described above and previous studies (*4*, *26*). This could be seen both from the iodide quenching (Figure 2A), which decreased under conditions favoring formation of the TM state, and 10-DN quenching (Figure 2B), which increased under these conditions. As shown by the quenching ratio (Figure 2C), the P345E, P345G, and P345N mutations all inhibited deep insertion of residues 356 and 311 in the TM state to some degree. However, the inhibition of deep insertion of residue 356 was smallest for the P345N mutation. The L307R mutation also decreased the depth of 311 and 356 insertion in the TM state to a significant degree. Thus, the quenching results basically agree well with the other

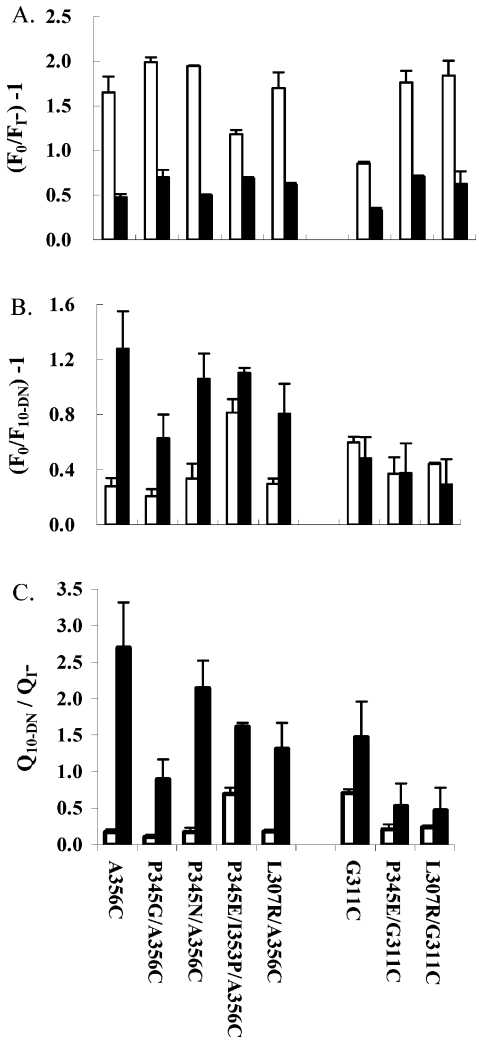

FIGURE 2: Iodide and 10-DN quenching of bimane labels on T domain single-cysteine mutants. Samples containing 70% PC/30% DOPG SUV (200 μM lipid with or without 10-DN, see the text for details) and 1 μg/mL bound T domain protein were prepared in Tris-acetate buffer at pH 4.5. Quenching of bimane fluorescence intensity in the presence of iodide (A) or 10-DN (B) was used to calculate the quenching ratios (C) under conditions inducing formation of the P state (DOPC-containing vesicles) (open bars) or favoring the TM state (DMoPC-containing vesicles) (closed bars). F_0 denotes the intensity of bimane fluorescence without the quencher, whereas F_{10-DN} and F_{I^-} represent the bimane fluorescence intensities in the presence of the 10-DN or iodide. Quenching by 10-DN (Q_{10-DN}) and iodide (Q_{I^-}) equals $(F_{10-DN}/F_0) - 1$ and $(F_{I^-}/F_0) - 1$, respectively. Mutants in A and B are in the same order as indicated on the *x* axis of C. For each quencher, average values and standard deviations were calculated from the data from two separate samples.

assays used in this paper. However, the effect of the L307R mutation upon the depth of insertion of residue 356 was larger than expected based on the results of the other assays.

The effect of quenching by iodide on emission wavelength was used to try to distinguish whether the lesser degree of insertion of the T domain with P345G and P345E mutations relative to the T domain that is wild type at position 345 reflected mutant T-domain molecules that insert somewhat less deeply than wild type in TM conditions or reflected a normal deep insertion but by a smaller fraction of mutant proteins relative to the wild type. If a subpopulation of mutant proteins inserted as deeply as the wild type, the emission wavelength of mutants in TM conditions should be more similar to the wild type in the presence of iodide. This is true because the iodide should preferentially quench the fluorescence of the shallowly inserting populations. Using bimane-labeled proteins on residue 356, this was not observed. Instead, the difference between the wild type and mutant emission was relatively unchanged, consistent with the mutants being able to less deeply insert than the wild-type protein in TM conditions (data not shown). This conclusion is consistent with previous studies showing that the P345E mutant forms pores with a smaller conductivity and more flickering (transient open/closing) behavior than wild-type proteins, both of which suggest an altered conformation relative to the wild type (*19*).

DISCUSSION

Using Multiple Assays To Evaluate the Structure of the Membrane-Inserted T Domain. Characterizing T-domain topography is challenging because the T domain is not a classical membrane protein. Its hydrophobic sequences are not as hydrophobic as those in usual membrane proteins, and therefore, it can form both deeply and shallowly inserting states when associated with lipid bilayers (*4*, *27*). Even when it inserts deeply, it has hydrophobic helices (TH5−7) that do not even form TM structures, at least under most conditions (*10*, *27*, *28*).

Our approach to this complexity has been to study the membrane-inserted T-domain structure with multiple techniques. Use of a single technique can be deceptive if it involves a parameter that depends on more variables than the one of interest. Using multiple assays that all depend on the desired variable can help to cancel out peculiarities encountered with just a single assay. An inevitable consequence of using multiple assays in this way is that they will occasionally give slightly different results. Conclusions based from studies using a single assay may appear better because, by definition, they avoid this possibility. However, this advantage is illusive: using a single assay, some results will simply be misleading. With multiple assays, conclusions that are supported by overall consensus of the data are much more robust than conclusions from a single assay.

Role of P345 in T-Domain Structure and Function. So far, Pro345 is one of the few DT residues that has been found to have a critical role in maintaining toxicity and pore formation. P345 sits at the tip of the loop between TH8 and TH9 in the solution structure of DT. Because TH8 and 9 form a TM hairpin crucial for both pore formation and translocation (*9*, *41*, *44*, *45*), it seems likely that Pro345 has a critical role in maintaining the normal TM hairpin structure.

Our studies show that T domains containing the P345E and P345G mutations do insert into the lipid bilayer but also show that the mutations reduce how deeply TH8 and 9 insert within the bilayer. This supports the proposal that Pro345 is important for normal insertion of these hydrophobic helices. The requirement for Pro at position 345 is relatively stringent, as shown by the inability of Pro at 347 or 353 to rescue mutations at position 345, and the inability of Gly, which like Pro can be a helix breaker, to fully substitute for Pro. The observation that substitution of Pro with Asn, the residue with the next strongest propensity to support turn formation had less deleterious effects on T-domain conformation as judged by iodide/10-DN quenching, pore formation, and antibody binding, suggests that promotion of turn formation is an important part of the function of P345. The inability of Asn to completely mimic Pro345 might partly be related to the fact Asn is less hydrophobic than Pro (*46*).

Relationship Between T-Domain Conformation and Pore Formation. In this paper, we found mutations that disrupt insertion of helix TH9 also disrupted pore formation but a mutation that disrupted helix TH7 insertion did not greatly inhibit pore formation. This is in agreement with previous data indicating that the TH8 and 9 hairpin has the primary role in pore formation by the T domain (*41*). However, it should be noted that we do not know if disruption of the insertion of helix TH5 would disrupt insertion of helices TH8 and 9, and therefore, we cannot rule out a role of helix TH5 in pore formation. In fact, a E295K mutation in the hydrophilic loop connecting TH5 to TH6 does inhibit pore formation (data not shown and ref *16*). Because this mutation is likely to affect the insertion of TH5, it may suggest that TH5 has some role in pore formation.

In a previous study, Zhan et al. found that the P345G mutation blocked pore formation in vesicles to a much higher degree than the P345E mutation as measured by an efflux assay (*19*). Our data indicate that the P345G only induced pore formation to a slightly lesser degree than P345E. We do not understand the origin of this difference, although differences in experimental conditions (e.g., pH) in our studies and that of Zhan et al. may be involved. We note that our data are self-consistent in the sense that both the degree of inhibition of deep insertion and inhibition of pore formation by P345E and P345G mutations is similar.

Advantages of the Biotin/BODIPY-SA Pore Assay. The biotin/BODIPY-SA pore assay introduced in this paper has several advantages. Influx processes with half-times over 15 s can easily be followed spectroscopically. Influx can be initiated at any time by the addition of the biotin-labeled molecule to the external solution. Thus, one can assay changes in pore properties after initial pore formation upon T-domain insertion. Such events cannot be assayed in efflux experiments, in which leakage starts as soon as the pore-forming molecule inserts into membranes. A final advantage of this protocol is its sensitivity. With a relatively high biotin concentration, the first few percent influx and an initial rate can easily be measured. When the size of the biotinylated molecule used is varied, it should also be possible to estimate pore size, at least when pores are not large enough to cause streptavidin leakage.

Interaction Between T-Domain Helices TH5−7 and Helices TH8 and 9 and the Structure of Membrane-Inserted T Domain in the TM State. Another important observation from

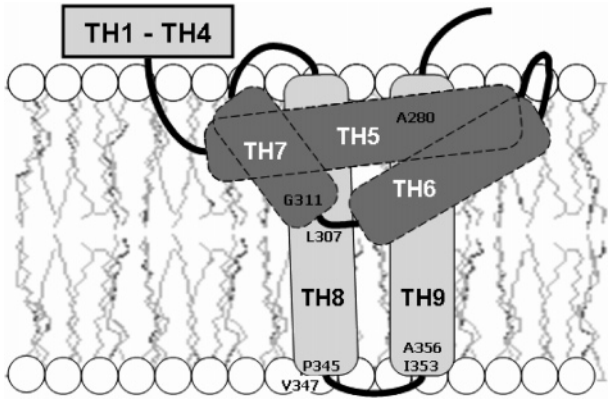

FIGURE 3: Schematic diagram of hypothetical topography of hydrophobic helices of T domain in the TM state. Hydrophobic helices TH8 and 9 are shown lightly shaded. Helices TH5−7 are shown darkly shaded. Residues studied or labeled in this paper are indicated. In the model shown, helices TH5−7 interact directly with helices TH8 and 9. A less likely alternative is that there is no direct interaction but that the insertion of helices TH8 and 9 is obligatory for insertion of helices TH5−7.

these studies concerns the linkage between conformational changes in the TH8 and 9 subdomain and that in the deeply inserting but non-TM TH5−7 region. Insertion of helices TH8 and 9 in the TM state clearly aids membrane penetration by helices TH5−7. Results showing that membrane penetration of helix TH7 has only a small effect on the insertion of helices TH8 and 9, while TH5−7 insertion is dependent upon the insertion of TH8 and 9, suggest the possibility that deep TH8 and 9 insertion precedes that of TH5−7, and thus, TH8 and 9 insertion may be an early step in T-domain insertion. These results also imply that the TH8 and 9 and TH5−7 subdomains are likely to be interacting with each other within the deeply membrane-inserted TM state rather than existing as two independent structures that are not in direct contact (Figure 3). If this is true, it is likely that helices TH5−7 have an important role in translocation. This role could involve forming a part of the pathway through which the A chain translocates or by being part of the toxin that actually crosses the membrane with the A chain (*10*, *13*). Indeed, a model that has been proposed for the T domain after translocation requires that TM insertion of helix TH5 takes place during the translocation process (*10*). Thus, further studies of the structure of helices TH5−7 during translocation, including their spacial relationship to TH8 and 9 and the effect of mutations that alter TH5−7 insertion, should yield important insights into the translocation process.

It should be noted that the effect of mixing wild-type and mutant proteins indicates that the interaction of TH5−7 with TH8 and 9 does not involve an intermolecular interaction between TH5−7 on one T-domain molecule and TH8 and 9 on another. If this interaction was primarily intermolecular, it would predict that the addition of excess wild-type protein could restore the normal insertion of TH5−7 that was within a molecule containing a mutation at Pro 345. This was not observed.

ACKNOWLEDGMENT

The authors would like to thank Jie Wang for helpful discussions.

REFERENCES

1. Choe, S., Bennett, M. J., Fujii, G., Curmi, P. M., Kantardjieff, K. A., Collier, R. J., and Eisenberg, D. (1992) The crystal structure of diphtheria toxin, *Nature 357*, 216−222.
2. Bennett, M. J., Choe, S., and Eisenberg, D. (1994) Refined structure of dimeric diphtheria toxin at 2.0 Å resolution, *Protein Sci. 3*, 1444−1463.
3. Zhan, H., Oh, K. J., Shin, Y. K., Hubbell, W. L., and Collier, R. J. (1995) Interaction of the isolated transmembrane domain of diphtheria toxin with membranes, *Biochemistry 34*, 4856−4863.
4. Wang, Y., Malenbaum, S. E., Kachel, K., Zhan, H., Collier, R. J., and London, E. (1997) Identification of shallow and deep membrane-penetrating forms of diphtheria toxin T domain that are regulated by protein concentration and bilayer width, *J. Biol. Chem. 272*, 25091−25098.
5. Collier, R. J. (2001) Understanding the mode of action of diphtheria toxin: A perspective on progress during the 20th century, *Toxicon 39*, 1793−1803.
6. Moskaug, J. O., Stenmark, H., and Olsnes, S. (1991) Insertion of diphtheria toxin B-fragment into the plasma membrane at low pH. Characterization and topology of inserted regions, *J. Biol. Chem. 266*, 2652−2659.
7. Ratts, R., Zeng, H., Berg, E. A., Blue, C., McComb, M. E., Costello, C. E., vanderSpek, J. C., and Murphy, J. R. (2003) The cytosolic entry of diphtheria toxin catalytic domain requires a host cell cytosolic translocation factor complex, *J. Cell Biol. 160*, 1139−1150.
8. Oh, K. J., Zhan, H., Cui, C., Altenbach, C., Hubbell, W. L., and Collier, R. J. (1999) Conformation of the diphtheria toxin T domain in membranes: A site-directed spin-labeling study of the TH8 helix and TL5 loop, *Biochemistry 38*, 10336−10343.
9. Finkelstein, A., Oh, K. J., Senzel, L., Gordon, M., Blaustein, R. O., and Collier, R. J. (2000) The diphtheria toxin channel-forming T-domain translocates its own NH2-terminal region and the catalytic domain across planar phospholipid bilayers, *Int. J. Med. Microbiol. 290*, 435−440.
10. Senzel, L., Gordon, M., Blaustein, R. O., Oh, K. J., Collier, R. J., and Finkelstein, A. (2000) Topography of diphtheria Toxin's T domain in the open channel state, *J. Gen. Physiol. 115*, 421−434.
11. Senzel, L., Huynh, P. D., Jakes, K. S., Collier, R. J., and Finkelstein, A. (1998) The diphtheria toxin channel-forming T domain translocates its own NH2-terminal region across planar bilayers, *J. Gen. Physiol. 112*, 317−324.
12. Lanzrein, M., Falnes, P. O., Sand, O., and Olsnes, S. (1997) Structure−function relationship of the ion channel formed by diphtheria toxin in vero cell membranes, *J. Membr. Biol. 156*, 141−148.
13. Ren, J., Kachel, K., Kim, H., Malenbaum, S. E., Collier, R. J., and London, E. (1999) Interaction of diphtheria toxin T domain with molten globule-like proteins and its implications for translocation, *Science 284*, 955−957.
14. Hu, H. Y., Huynh, P. D., Murphy, J. R., and vanderSpek, J. C. (1998) The effects of helix breaking mutations in the diphtheria toxin transmembrane domain helix layers of the fusion toxin DAB389IL-2, *Protein Eng. 11*, 811−817.
15. Cabiaux, V., Mindell, J., and Collier, R. J. (1993) Membrane translocation and channel-forming activities of diphtheria toxin are blocked by replacing isoleucine 364 with lysine, *Infect. Immun. 61*, 2200−2202.
16. Falnes, P. O., Madshus, I. H., Sandvig, K., and Olsnes, S. (1992) Replacement of negative by positive charges in the presumed membrane-inserted part of diphtheria toxin B fragment. Effect on membrane translocation and on formation of cation channels, *J. Biol. Chem. 267*, 12284−12290.
17. Johnson, V. G., Nicholls, P. J., Habig, W. H., and Youle, R. J. (1993) The role of proline 345 in diphtheria toxin translocation, *J. Biol. Chem. 268*, 3514−3519.
18. Silverman, J. A., Mindell, J. A., Finkelstein, A., Shen, W. H., and Collier, R. J. (1994) Mutational analysis of the helical hairpin region of diphtheria toxin transmembrane domain, *J. Biol. Chem. 269*, 22524−22532.
19. Zhan, H., Elliott, J. L., Shen, W. H., Huynh, P. D., Finkelstein, A., and Collier, R. J. (1999) Effects of mutations in proline 345 on insertion of diphtheria toxin into model membranes, *J. Membr. Biol. 167*, 173−181.

20. Cabiaux, V., Quertenmont, P., Conrath, K., Brasseur, R., Capiau, C., and Ruysschaert, J. M. (1994) Topology of diphtheria toxin B fragment inserted in lipid vesicles, *Mol. Microbiol. 11*, 43−50.
21. Madshus, I. H., Wiedlocha, A., and Sandvig, K. (1994) Intermediates in translocation of diphtheria toxin across the plasma membrane, *J. Biol. Chem. 269*, 4648−4652.
22. Mindell, J. A., Zhan, H., Huynh, P. D., Collier, R. J., and Finkelstein, A. (1994) Reaction of diphtheria toxin channels with sulfhydryl-specific reagents: Observation of chemical reactions at the single molecule level, *Proc. Natl. Acad. Sci. U.S.A. 91*, 5272−5276.
23. Zhan, H., Choe, S., Huynh, P. D., Finkelstein, A., Eisenberg, D., and Collier, R. J. (1994) Dynamic transitions of the transmembrane domain of diphtheria toxin: Disulfide trapping and fluorescence proximity studies, *Biochemistry 33*, 11254−11263.
24. Oh, K. J., Zhan, H., Cui, C., Hideg, K., Collier, R. J., and Hubbell, W. L. (1996) Organization of diphtheria toxin T domain in bilayers: A site-directed spin labeling study, *Science 273*, 810−812.
25. Quertenmont, P., Wattiez, R., Falmagne, P., Ruysschaert, J. M., and Cabiaux, V. (1996) Topology of diphtheria toxin in lipid vesicle membranes: A proteolysis study, *Mol. Microbiol. 21*, 1283−1296.
26. Kachel, K., Ren, J., Collier, R. J., and London, E. (1998) Identifying transmembrane states and defining the membrane insertion boundaries of hydrophobic helices in membrane-inserted diphtheria toxin T domain, *J. Biol. Chem. 273*, 22950−22956.
27. Rosconi, M. P., and London, E. (2002) Topography of helices 5−7 in membrane-inserted diphtheria toxin T domain: Identification and insertion boundaries of two hydrophobic sequences that do not form a stable transmembrane hairpin, *J. Biol. Chem. 277*, 16517−16527.
28. Rosconi, M. P., Zhao, G., and London, E. (2004) Analyzing topography of membrane-inserted diphtheria toxin T domain using BODIPY-streptavidin: At low pH, helices 8 and 9 form a transmembrane hairpin but helices 5−7 form stable nonclassical inserted segments on the cis side of the bilayer, *Biochemistry 43*, 9127−9139.
29. Petros, A. M., Medek, A., Nettesheim, D. G., Kim, D. H., Yoon, H. S., Swift, K., Matayoshi, E. D., Oltersdorf, T., and Fesik, S. W. (2001) Solution structure of the antiapoptotic protein bcl-2, *Proc. Natl. Acad. Sci. U.S.A. 98*, 3012−3017.
30. Parker, M. W., Postma, J. P., Pattus, F., Tucker, A. D., and Tsernoglou, D. (1992) Refined structure of the pore-forming domain of colicin A at 2.4 Å resolution, *J. Mol. Biol. 224*, 639−657.
31. Schinzel, A., Kaufmann, T., Schuler, M., Martinalbo, J., Grubb, D., and Borner, C. (2004) Conformational control of Bax localization and apoptotic activity by Pro168, *J. Cell. Biol. 164*, 1021−1032.
32. Bradford, M. M. (1976) A rapid and sensitive method for the quantitation of microgram quantities of protein utilizing the principle of protein-dye binding, *Anal. Biochem. 72*, 248−254.
33. Caputo, G. A., and London, E. (2003) Using a novel dual fluorescence quenching assay for measurement of tryptophan depth within lipid bilayers to determine hydrophobic α-helix locations within membranes, *Biochemistry 42*, 3265−3274.
34. Hayashibara, M., and London, E. (2005) Topography of diptheria toxin A chain inserted into lipid vesicles, *Biochemistry 44*, 2183−2196.
35. Ren, J., Lew, S., Wang, Z., and London, E. (1997) Transmembrane orientation of hydrophobic α-helices is regulated both by the relationship of helix length to bilayer thickness and by the cholesterol concentration, *Biochemistry 36*, 10213−10220.
36. Batzri, S., and Korn, E. D. (1973) Single bilayer liposomes prepared without sonication, *Biochim. Biophys. Acta 298*, 1015−1019.
37. Jiang, J. X., Chung, L. A., and London, E. (1991) Self-translocation of diphtheria toxin across model membranes, *J. Biol. Chem. 266*, 24003−24010.
38. Nilsson, I., and von Heijne, G. (1998) Breaking the camel's back: Proline-induced turns in a model transmembrane helix, *J. Mol. Biol. 284*, 1185−1189.
39. Monne, M., Nilsson, I., Elofsson, A., and von Heijne, G. (1999) Turns in transmembrane helices: Determination of the minimal length of a "helical hairpin" and derivation of a fine-grained turn propensity scale, *J. Mol. Biol. 293*, 807−814.
40. Oh, K. J., Senzel, L., Collier, R. J., and Finkelstein, A. (1999) Translocation of the catalytic domain of diphtheria toxin across planar phospholipid bilayers by its own T domain, *Proc. Natl. Acad. Sci. U.S.A. 96*, 8467−8470.
41. Silverman, J. A., Mindell, J. A., Zhan, H., Finkelstein, A., and Collier, R. J. (1994) Structure−function relationships in diphtheria toxin channels: I. Determining a minimal channel-forming domain, *J. Membr. Biol. 137*, 17−28.
42. Sharpe, J. C., and London, E. (1999) Diphtheria toxin forms pores of different sizes depending on its concentration in membranes: Probable relationship to oligomerization, *J. Membr. Biol. 171*, 209−221.
43. Emans, N., Biwersi, J., and Verkman, A. S. (1995) Imaging of endosome fusion in BHK fibroblasts based on a novel fluorimetric avidin−biotin binding assay, *Biophys. J. 69*, 716−728.
44. Huynh, P. D., Cui, C., Zhan, H., Oh, K. J., Collier, R. J., and Finkelstein, A. (1997) Probing the structure of the diphtheria toxin channel. Reactivity in planar lipid bilayer membranes of cysteine-substituted mutant channels with methanethiosulfonate derivatives, *J. Gen. Physiol. 110*, 229−242.
45. Mindell, J. A., Silverman, J. A., Collier, R. J., and Finkelstein, A. (1994) Structure−function relationships in diphtheria toxin channels: III. Residues which affect the cis pH dependence of channel conductance, *J. Membr. Biol. 137*, 45−57.
46. Kyte, J., and Doolittle, R. F. (1982) A simple method for displaying the hydropathic character of a protein, *J. Mol. Biol. 157*, 105−132.

BI047705O